Science of the Total Environment 650 (2019) 1944–1953

Contents lists available at ScienceDirect

Science of the Total Environment

journal homepage: www.elsevier.com/locate/scitotenv

A modeling study of the peroxyacetyl nitrate (PAN) during a wintertime haze event in Beijing, China

Yulu Qiu [a,b,c], Zhiqiang Ma [a,b,*], Ke Li [d]

[a] Institute of Urban Meteorology, China Meteorological Administration, Beijing 100089, China
[b] Beijing Shangdianzi Regional Atmosphere Watch Station, Beijing, China
[c] Key Laboratory of Atmospheric Chemistry, China Meteorological Administration, Beijing 100081, China
[d] John A. Paulson School of Engineering and Applied Sciences, Harvard University, Cambridge, MA 02138, USA

HIGHLIGHTS

- The CBM-Z scheme performed much better in simulating PAN concentrations.
- A 20% increase in VOC emissions could lead to 45% increase in PAN concentrations.
- Local sources accounted for 15%–30% of PAN concentrations over most of Beijing.

GRAPHICAL ABSTRACT

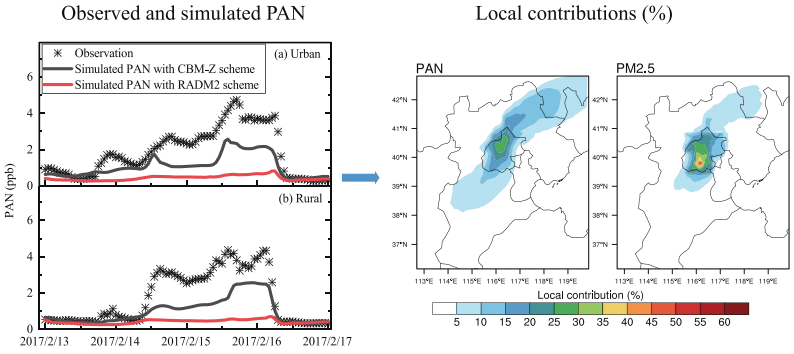

ARTICLE INFO

Article history:
Received 23 July 2018
Received in revised form 17 September 2018
Accepted 19 September 2018
Available online 21 September 2018

Editor: Pavlos Kassomenos

Keywords:
PAN
WRF-Chem
Beijing
Haze event

ABSTRACT

Peroxyacetyl nitrate (PAN), as the second most important photochemical pollutant, could threaten human health and terrestrial ecosystem. Observed high PAN concentrations in wintertime in Beijing are comparable to those in summertime when photochemistry is strong. In this study, we investigated the variations of concentrations of PAN and other related chemical species during a haze event on February 13–16, 2017 in Beijing using a combination of in-situ observations and the WRF-Chem model simulation. During this episode, the observed mean (maximum) PAN concentrations at the urban and rural sites were 1.9 (4.7) ppb and 1.8 (4.3) ppb, respectively. Model evaluation showed that the simulation with CBM-Z gas-phase scheme performed much better than simulation using the RADM2 scheme, which mainly results from the accurate representation of the reaction rates for PAN formation through $CH_3C(O)O_2$ radicals and NO_2 in the CBM-Z scheme. But simulated PAN concentrations in Beijing were still underpredicted using the CBM-Z scheme, likely due to the underestimation of VOC emissions. Since the lifetime of PAN becomes as long as several days in wintertime due to lower temperature, it could be conducive to be accumulated and transported. Sensitivity simulation demonstrated that local sources accounted for about 15%–30% of mean PAN concentrations over most of Beijing during the event, lower than that of $PM_{2.5}$ (25%–60%). These suggest that during Beijing wintertime polluted days, increased PAN concentration, which is dominantly contributed by regional transport from surrounding areas, will cause more health concerns, and its control strategies need larger regional efforts than those conducted for $PM_{2.5}$.

* Corresponding author at: Institute of Urban Meteorology, China Meteorological Administration, Beijing 100089, China.
E-mail address: zqma@ium.cn (Z. Ma).

https://doi.org/10.1016/j.scitotenv.2018.09.253
0048-9697/

1. Introduction

Peroxyacetyl nitrate (PAN), formed through the photochemical reactions between volatile organic compounds (VOCs) and NO_x, is usually considered as the second most important photochemical pollutant (Stephens, 1969; Singh and Salas, 1989; Fischer et al., 2014). High PAN levels could lead to plant injury (Taylor, 1969; Temple and Taylor, 1983) and threaten human health (Heuss and Glasson, 1968). The primary removal process for PAN in the lower troposphere is thermal decomposition (Seinfeld and Pandis, 2006), resulting in longer lifetime with lower temperature. Therefore, PAN has been identified as the reservoir for both $CH_3C(O)O_2$ radicals and NO_x, which can induce long-distance transport (Nielsen et al., 1981; Singh et al., 1986) and release NO_x in those regions with higher temperature (Singh et al., 1992; Suppana et al., 1998; Hudman et al., 2004), influencing the formation of ozone (O_3) in those areas. Beijing, as the capital city of China, has undergone rapid development of economy and urbanization over past three decades, also along with the severe atmospheric environment concerns (Wang et al., 2014; Ma et al., 2016; Cai et al., 2017; Qiu et al., 2017). Especially, Ma et al. (2016) reported that measured ozone concentration in rural Beijing has undergone a significant increase in the period of 2003–2015, with an average rate of 1.13 ± 0.01 ppb $year^{-1}$, implying that the photochemical pollution has become serious in this region. As the second important photochemical pollutant, it is of great importance to investigate PAN's features in Beijing and will also deepen our understanding of the photochemical levels in this region.

Many observational studies investigated the formation processes (J.M. Zhang et al., 2009; Zhang et al., 2011; Xue et al., 2014; Xu et al., 2015) and relationships with other chemical species (Zhang et al., 2014; Zhang et al., 2017) for PAN in China. For example, J.M. Zhang et al. (2009) reported that pollution events with high PAN mixing ratios at the background site of Waliguan (260 km away from Lanzhou) were substantially influenced by the air mass from Lanzhou (urban area). By analyzing observations from a background site in the Pearl River Delta region during late summer and late autumn of 2011, Xu et al. (2015) showed that there existed strong positive correlation between simultaneous data of PAN versus O_3 with r^2 of 0.71–0.99. However, most of the above-mentioned studies focused on PAN pollution in summer when photochemical activities are strong, only a few studies paid attention to wintertime PAN pollution in China. Since the thermal decomposition of PAN is strongly dependent on temperature, wintertime PAN becomes more conducive to be accumulated and transported, and thus could survive as long as several days (Beine and Krognes, 2000). Zhang et al. (2014) pointed out that measured wintertime PAN concentrations in urban Beijing were negatively correlated with O_3; namely, PAN was conducive to be accumulated in the cold and stable atmosphere in wintertime. Frequent haze pollution events were observed in the North China Plain (NCP) in winter during recent years (Wang et al., 2014; Sun et al., 2016), which are mainly caused by the combination of anthropogenic emissions (Liu et al., 2016), terrain effects (Zhang et al., 2018), the stable atmospheric conditions (Zheng et al., 2015; Cai et al., 2017; Li et al., 2018), regional transport (Yang et al., 2017a) and aerosol-meteorology interactions (Yang et al., 2017b). High PAN concentrations are also observed during such haze episodes in this study, which will cause more health concerns, and it is pressing to understand the cause.

A few of modeling studies have been conducted worldwide to simulate the evolution processes of PAN (Sudo et al., 2002; Singh et al., 2007; Fischer et al., 2014). For example, Singh et al. (2007) utilized three global chemical models (GEOS-Chem, RAQMS, MOZART) and one regional chemistry transport model (STEM) to simulate vertical distribution of PAN and other related species in North America, and found that only GEOS-Chem and RAQMS showed good performance in PAN simulation. Fischer et al. (2014) reported that global GEOS-Chem model could capture the major features of the existing PAN observations, but underprediction of PAN concentrations was also found in China and Europe. However, because of the lack of PAN observations, there were few regional modeling studies evaluating model performance in reproducing the variations of PAN levels during pollution events in China, to complement the understanding of the high PAN concentrations in this region. Besides, regional chemical models (e.g., WRF-Chem, CMAQ) have demonstrated good performance in simulating the variations of aerosols during the polluted events in the NCP (Gao et al., 2014; Gao et al., 2015; Ding et al., 2016; Gao et al., 2016; Li and Han, 2016; Qiu et al., 2017). It is, therefore, imperative to evaluate the performance of these models in simulating PAN, taking advantage of in-situ observations of PAN and other related chemical species.

In this study, we present the measured concentrations of PAN and other chemical species in Beijing during February 13 to 17, 2017 and conduct simulations of PAN using the WRF-Chem model to evaluate the model performance and examine the cause of the pollution events with high PAN levels. The paper is organized as follows: The observational data and WRF-Chem model used in the study are described in Section 2. Section 3 presents the measured data for PAN and other related species, compares simulated meteorological and chemical variables with observations, and shows the contribution of local sources and regional transport to PAN concentrations in Beijing. The conclusion is presented in Section 4.

2. Observation data and model configuration

2.1. Observation data

Meteorological and chemical data are used to determine the pollution event and evaluate the predictions of PAN concentration during the event. In this study, the surface-layer PAN concentration is measured by on-line gas chromatography equipped with electron capture detector (GC-ECD), with a time resolution of 5 min. There are two stations for PAN measurement. The Baolian station (BL, 39°56′N, 116°17′E, 75.0 m a.s.l.) represents the urban region, which is located between the west 3rd and 4th ring road of downtown Beijing. The Shangdianzi station (SDZ, 40°39′N, 117°07′E, 293.9 m a.s.l.) is one of the regional Global Atmosphere Watch (GAW) stations in China, which is located in the northern part of the NCP, about 100 km northeast of the BL station. The measurement was conducted during the whole year of 2016–2017. The detailed locations of the two sites are presented in Fig. S1. Hourly concentrations of $PM_{2.5}$, NO_2 and O_3 in Beijing are obtained from the China National Environmental Monitoring Center (CNEMC). Data from twelve CNEMC stations in Beijing are used, and the detailed information of these stations have been listed in Table S1.

Surface meteorological data are obtained from the China Meteorological Administration (CMA), which consist of temperature at 2 m (T2), relative humidity at 2 m (RH2), sea level pressure (SLP), wind speed at 10 m (WS10), and wind direction at 10 m (WD10). The data in Nanjiao Station (39.8°N, 116.47°E, 55.0 m a.s.l.) are utilized here to represent the surface meteorological features in urban Beijing. The radiosonde data in Beijing (39.93°N, 116.28°E, 55.0 m a.s.l), collected by the University of Wyoming, Department of Atmospheric Science (http://weather.uwyo.edu/upperair/sounding.html), are also used to evaluate the simulated temperature profiles.

2.2. WRF-Chem model

The atmospheric chemical transport model used in this study is the WRF-Chem 3.6.1 version, which simulates the variations of atmospheric chemical species and meteorological fields simultaneously (Grell et al., 2005; Fast et al., 2006; Chapman et al., 2009). Fig. S1 also presents the setup of the model domain in this study, which covers the whole

areas of the northern China, with the horizontal resolution of 9 km. The model is configured with 30 vertical layers up to 50 hPa.

The chemical parameterization schemes used in this study consist of the Regional Acid Deposition Model version 2 (RADM2) gas scheme (Stockwell et al., 1990) coupled with the Modal Aerosol Dynamics Model for Europe and Secondary Organic Aerosol Model (MADE/SORGAM) (Ackermann et al., 1998; Schell et al., 2001), and the CBM-Z gas scheme (Zaveri and Peters, 1999) with the Model for Simulating Aerosol Interactions and Chemistry (MOSAIC) (Zaveri et al., 2008) with four sizes of bins. Dry depositions of trace gases and aerosol particles are both included in the two sets of the chemical schemes, which are based on the methods of Wesely (1989) and Binkowski and Shankar (1995), respectively. The physical schemes include the WSM 6-class microphysics scheme (Hong and Lim, 2006), Goddard shortwave radiation scheme (Chou et al., 1998), RRTM longwave radiation scheme (Mlawer et al., 1997), and Yonsei University boundary layer scheme (Hong et al., 2006).

The (Multi-resolution Emission Inventory for China) MEIC emission inventory for 2012 (http://www.meicmodel.org) developed by Tsinghua University (Q. Zhang et al., 2009; Li et al., 2014; Zheng et al., 2014; Liu et al., 2015) is utilized here. This inventory consists of anthropogenic emission rates of SO_2, NO_x, CO, NH_3, NMVOC, black carbon (BC), primary organic carbon (POC), primary $PM_{2.5}$ and PM_{10}, which is divided into five sectors (industry, energy, residential, transportation and agriculture) for each species. This inventory has been widely applied to simulate the haze event in China (Zhang et al., 2015; Qiu et al., 2017). The emission rates in February are used and the hourly scale factors in each sector are shown in Fig. S2. As we utilize emissions in 2012 to simulate the distribution of pollutants in 2017, there may exist uncertainties since emissions would change during 2012–2017. Biogenic emissions are calculated from the Model of Emissions of Gases and Aerosols from Nature (MEGAN) (Guenther et al., 2006).

2.3. Experimental design

To examine the performance of the gas schemes in the WRF-Chem model in simulating the variations of PAN and other chemical species, and to investigate the contribution of local sources and regional transport to the PAN levels in Beijing during wintertime pollution events, we conducted the following simulations:

1) CTRL_CBMZ case: The control simulation with the standard emissions using the CBM-Z gas scheme.
2) CTRL_RADM2 case: The simulation with the standard emissions but using the RADM2 gas scheme.
3) NOBJ_CBMZ case: The same as the CTRL_CBMZ case, except that all the emissions in Beijing were turned off.
4) CTRL_1.2VOC case: The same as the CTRL_CBMZ case, except that VOC emissions were increased by 20%.

The first two simulations are used to assess the model performance using two different gas schemes. The CBM-Z and RADM2 schemes are two widely-used schemes in WRF-Chem. The comparison with observation results could help us choose the chemical schemes which are suitable for the simulation of PAN in the study area. The difference between the CTRL_CBMZ and NOBJ_CBMZ cases represents the contribution of local sources to PAN concentrations in Beijing. In addition, we also conducted the CTRL_1.2VOC case to figure out possible reason of the underestimated PAN concentration in the model. The simulation period was from February 12, 2017 to February 17, 2017, when the NCP was suffering a severe haze event. All of the simulations use the same initial and boundary meteorological conditions provided by the National Centers for Environmental Prediction (NCEP) $1° \times 1°$ reanalysis data. The corresponding conditions for chemical species are from the results of the Model for Ozone and Related chemical Tracers, version 4 (MOZART-4) (Emmons et al., 2010).

3. Results and discussion

3.1. Observed PAN and $PM_{2.5}$ pollution event

The time series of observed concentrations of PAN and $PM_{2.5}$ at the rural (SDZ) and urban sites (BL) in Beijing during the wintertime of 2016–2017 are displayed in Fig. 1. The measured daily maximum

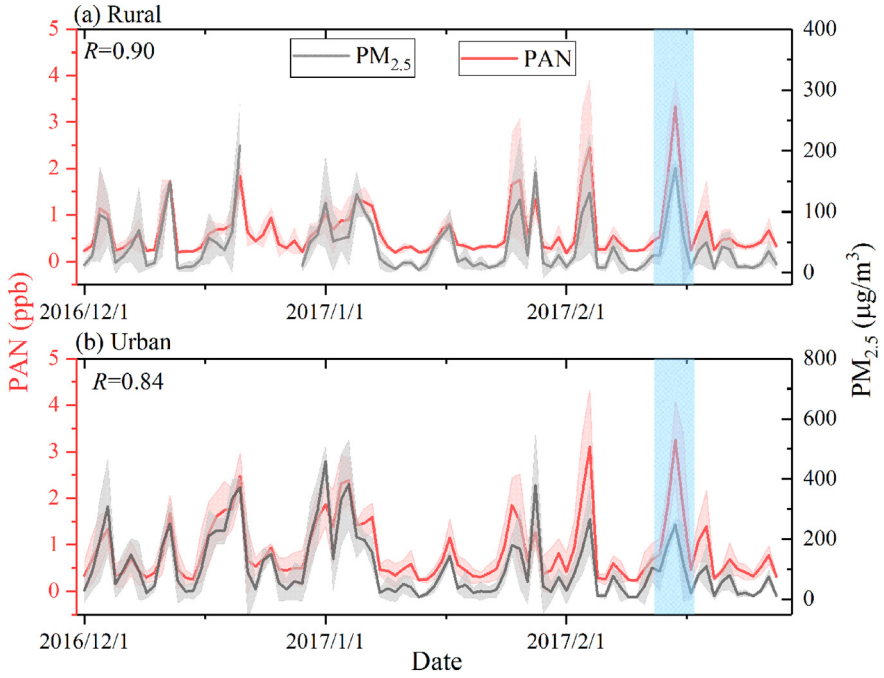

Fig. 1. Observed daily concentrations of PAN (ppb) and $PM_{2.5}$ ($\mu g/m^3$) at the rural (a) and urban sites (b) during winter of 2016–2017. The standard deviation is calculated by the hourly data and displayed by shades. Blue rectangular shades denotes the simulation periods in this study.

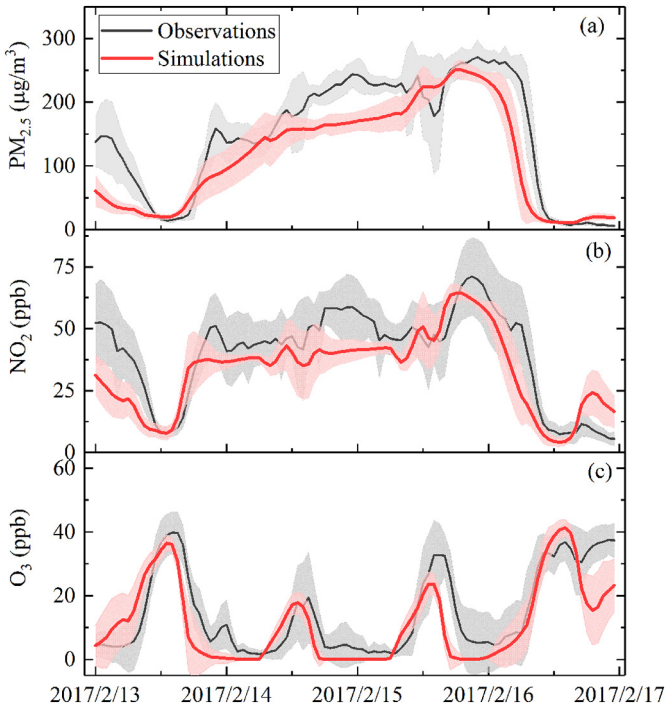

Fig. 2. Time series of simulated (CTRL_CBMZ, red) and observed (black) concentrations of $PM_{2.5}$ (μg/m^3), NO_2 (ppb) and O_3 (ppb) averaged over 12 stations from CNEMC in Beijing during February 13–17, 2017. The standard deviation is calculated by the observed and simulated results in 12 CNMEC stations and displayed by shades.

concentrations for PAN at the urban and rural sites reached 3.3 ppb and 3.2 ppb, respectively; the hourly maximum values for the two sites were 4.7 ppb and 4.3 ppb, respectively. The observed high PAN levels in wintertime of Beijing were even comparable to those in summertime of China (Wang et al., 2010; Xu et al., 2015), when solar radiation was relatively strong and intensive. Moreover, there was good positive correlation between concentrations of PAN and $PM_{2.5}$ in winter at both of the two sites; namely, the high PAN levels usually coincided with the haze events in winter. To better understand the evolution process of high PAN during haze events, atmospheric chemistry transport model is utilized in this study. We choose the widely used WRF-Chem model to simulate the high PAN levels in Beijing. The event was during February 13 to 16 (blue shades in Fig. 1), when the PAN concentrations at the two sites were both the highest during winter of 2016–2017.

3.2. Simulated concentrations of PAN and other chemical species

Fig. 2 shows the simulated (CTRL_CMBZ) and observed time series of concentrations for $PM_{2.5}$, NO_2 and O_3 in Beijing during February 13–17, 2017. The observed surface-layer concentrations of $PM_{2.5}$, NO_2 and O_3 from CNEMC averaged over 12 stations in Beijing were used. The

Table 1
Statistical performance of the simulated concentrations in the chemical species. Simulated concentrations are from the CTRL_CBMZ simulation, and PAN concentrations from the CTRL_RADM2 simulation are also given in brackets.

	OBS	SIM	MB	NMB	*R*
$PM_{2.5}$ (μg/m^3)	148.1	115.7	−32.4	−21.9%	0.90
NO_2 (ppb)	39.9	33.2	−6.7	−16.8%	0.84
O_3 (ppb)	14.9	11.4	−3.5	−23.5%	0.82
PAN (urban, ppb)	1.9	1.1 (0.4)	−0.8 (−1.3)	−42.1% (−68.4%)	0.93 (0.89)
PAN (rural, ppb)	1.7	1.0 (0.4)	−0.7 (−1.3)	−41.2% (−76.5%)	0.91 (0.81)

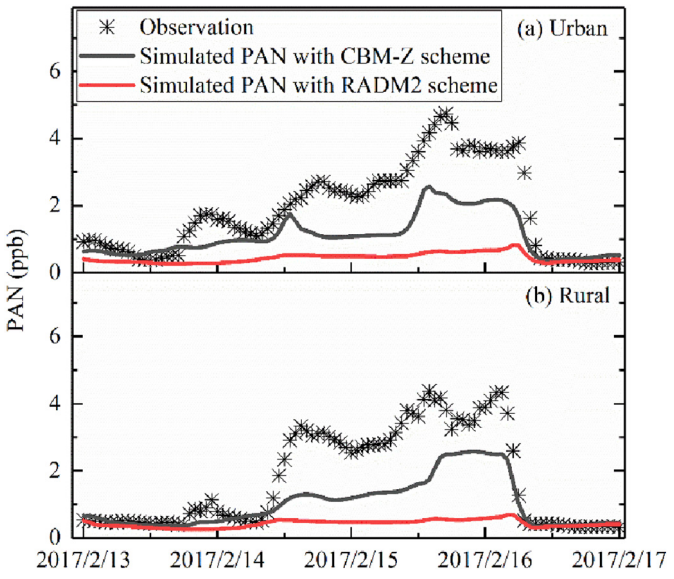

Fig. 3. Hourly time series of observed and simulated (CTRL_CMBZ and CTRL_RADM2) PAN concentrations (ppb) at the urban and rural sites in Beijing during February 13–17, 2017.

pollution event started from the nighttime of February 13 with rapid increase in $PM_{2.5}$ and NO_2 concentrations, and ended in the morning of February 16. The observed peak values of $PM_{2.5}$ and NO_2 concentrations during the pollution event were 271 μg/m^3 and 71 ppb, respectively. For O_3, it showed decrease in concentrations during the pollution event, which could be attributed to decreased solar radiation with high aerosol loadings, leading to reduced photolysis rate of O_3 formation and enhanced loss of HO_x (Gao et al., 2016; Qiu et al., 2017). In general, the model well captured observed pollution episode, although the magnitudes of the pollution might be underestimated to some extent. Table 1 summarizes the statistical results of the observed and simulated chemical concentrations in Beijing during the event. The statistical factors used in this study consist of mean bias (MB), normalized mean bias (NMB), and correlation coefficient (*R*). The model can reproduce the temporal variation of the event with *R* values of 0.90 for $PM_{2.5}$, 0.84 for NO_2 and 0.82 for O_3, respectively, but underestimate the concentrations with the MB values of −21.9%, −16.8%, and −23.5%, respectively. Previous studies revealed that the aerosol direct radiative effects during haze events in China could reduce the shortwave radiation near the surface, resulting in more stable boundary layer and increased

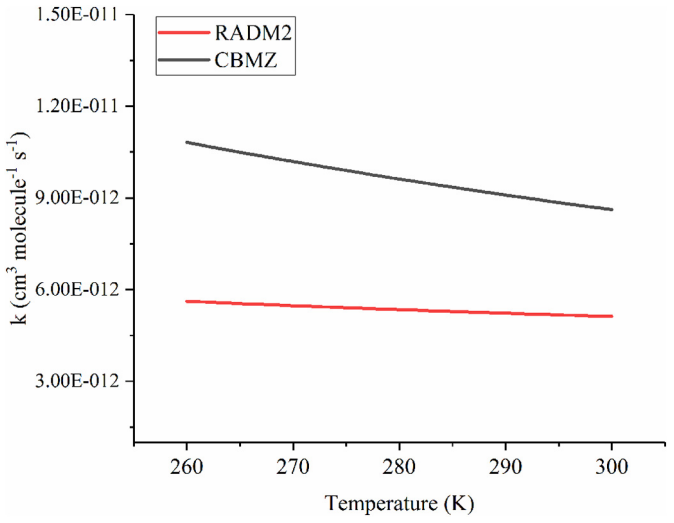

Fig. 4. Simulated reaction rate coefficients for the PAN formation through $CH_3C(O)O_2$ radicals and NO_2 in the function of temperature using the RADM2 and CBM-Z schemes.

Table 2
Statistical performance of the simulated meteorological variables from the CTRL_CBMZ simulation.

	OBS	SIM	MB	NMB	*R*
T2 (°C)	3.0	3.9	0.9	30.0%	0.90
RH2 (%)	49.9	58.4	8.5	17.0%	0.75
SLP (hPa)	1026.2	1026.3	0.1	~0	0.99
WS (m/s)	2.1	2.5	0.4	19.0%	0.81

surface pollutant concentrations (Wang et al., 2014; Gao et al., 2015; Ding et al., 2016; Qiu et al., 2017). This underestimation in this study might be the result of the exclusion of the aerosol radiative effects in the simulation.

Fig. 3 displays the temporal variations of observed and simulated surface-layer PAN concentrations at the urban and rural sites in Beijing during February 13–17. Measured PAN concentrations at the two sites began to rise in the nighttime of February 13 and showed a sharp decrease in the morning of February 16, coincided with that of $PM_{2.5}$. The maximum concentrations at the urban and rural sites reached 4.7 ppb and 4.3 ppb, respectively. We also calculated the lifetime of PAN against thermal decomposition by the method described in the CBM-Z scheme and Sander et al. (2006). Statistical results indicated that during February 13–17, the simulated lifetime of PAN against thermal decomposition was in the range of 6–102 h, with the mean value of 34.9 h. Therefore, under the low temperature, PAN can be more stable due to the low activity of thermal decomposition, which agrees well with the results in Beine and Krognes (2000). Besides, the positive correlation between PAN and $PM_{2.5}$ in winter (Fig. 1) also confirms the long lifetime of PAN, which is much different from other photochemical species, like O_3.

The comparisons between simulations using two chemical schemes and observations for PAN (Fig. 3) demonstrated that the two simulated results for PAN exhibited large differences in magnitude. The mean concentrations of PAN averaged during the event at the urban and rural sites using CBM-Z scheme were 1.1 ppb and 1.0 ppb, while the corresponding values for RADM2 scheme were decreased to 0.4 ppb and 0.4 ppb. Besides, CTRL_CBMZ simulation showed a higher positive correlation with observations than CTRL_RADM2 simulation. As described above, $CH_3C(O)O_2$ (PA) radicals react with NO_2 to form PAN (Eq. (1)), and PAN thermally decomposes back to precursors in turn (Eq. (2)):

$$CH_3C(O)O_2 + NO_2 + M \xrightarrow{1} CH_3C(O)O_2NO_2 + M \quad (1)$$

$$CH_3C(O)O_2NO_2 + M \xrightarrow{2} CH_3C(O)O_2 + NO_2 + M \quad (2)$$

PAN levels are highly determined by reaction rates of Eqs. (1) and (2), which are calculated through k_1[PA][NO_2] and k_2[PAN], respectively. Here, k_1 and k_2 are the reaction rate coefficients. In the CBM-Z

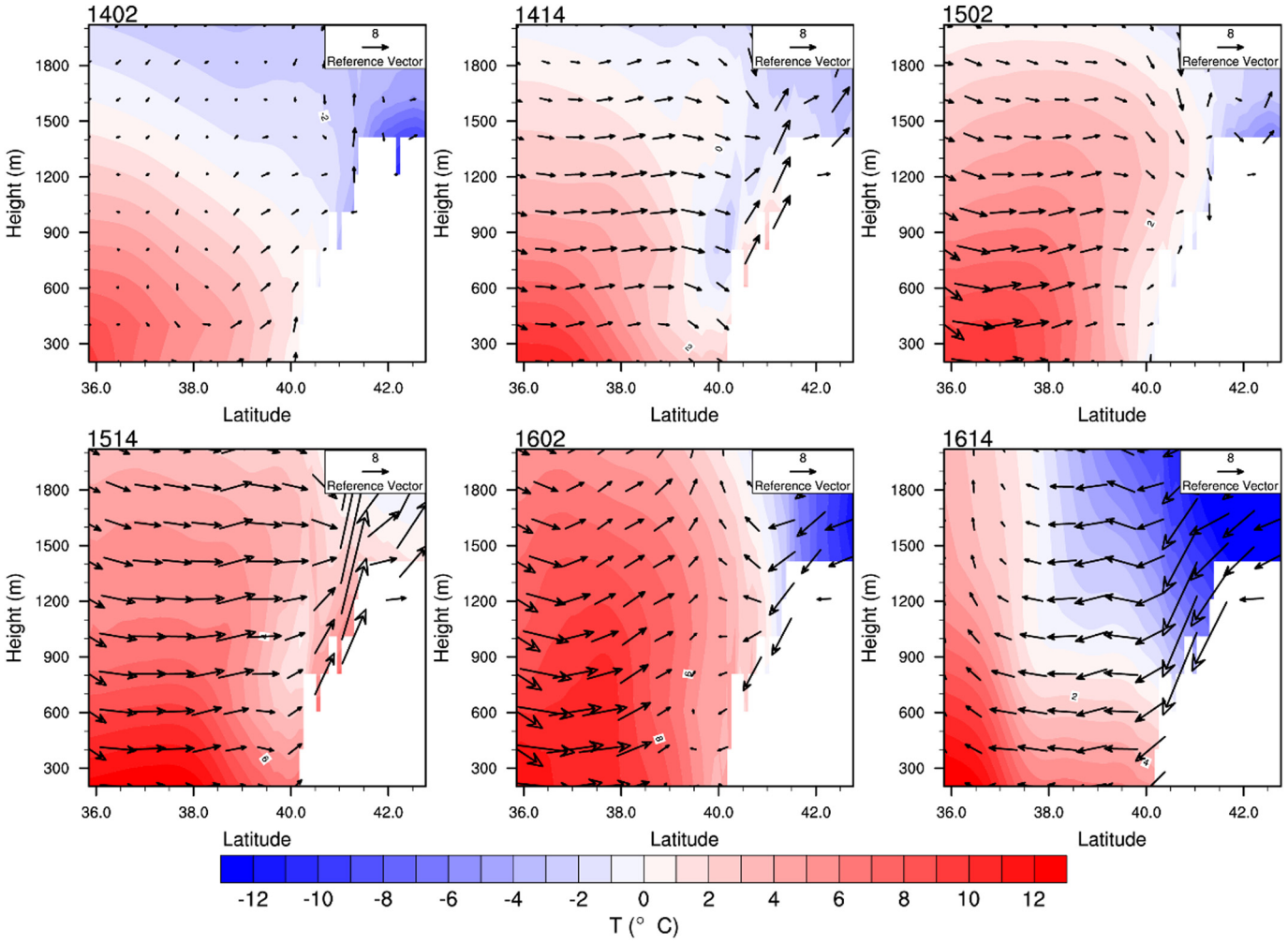

Fig. 5. Simulated N-S vertical cross sections of 12-hourly *v*-*w* wind components (vectors, m/s) and temperature (contours, °C) in the NCP along 116.4°E during February 14–16, 2017. The *w* wind component is multiplied by 100.

and RADM2 scheme, reaction rate coefficients for the PAN formation are calculated following Sander et al. (2006) and Stockwell et al. (1990), respectively. Considering that the two schemes utilize different methods in calculating k, there exist large discrepancies in the reaction rates and simulated PAN concentrations. Fig. 4 shows the variations of k_1 in the function of temperature using the two schemes, suggesting that the rates in the CTRL_CBMZ simulation are 70%–93% higher than those in the CTRL_RADM2 simulation. This could explain the discrepancy between the two schemes to some extent.

Although the CBM-Z scheme performs better than the RADM2 scheme, it still has low bias in simulated PAN concentrations compared with observations, with NMB values of −42.1% and −41.2% at the two sites. This underestimation was also reported in Fischer et al. (2014), which implied that low bias for PAN in China was largely attributed to the uncertainties in NMVOC emissions. Further sensitivity simulations (Fig. S3) show that a 20% increase in VOC emissions (CTRL_1.2VOC/CTRL_CBMZ) could lead to 45% increase in PAN concentrations, suggesting that the simulated variations of PAN are very sensitive to the VOC emissions in Beijing and its surrounding area. Therefore, accurate representation of VOC emissions is of great importance for the simulation of PAN. More importantly, such comparisons between in-situ measurement and model simulation of PAN may offer another approach to provide quantitative constraints on anthropogenic VOC emissions. Except for the underestimation of VOC emissions, it should be noted that the uncertainties in simulated meteorology, representations of the physical and chemical processes in the model, and interannual variations in emission rates could also lead to the bias between observation and simulation.

3.3. Simulated meteorological fields

The temporal variations of simulated and observed surface meteorological parameters in Beijing during this event are presented in Fig. S4. As discussed in Section 3.2, the CTRL_CBMZ simulation performs better, thus we utilize this simulation hereafter. The observed RH started to rise in the nighttime of February 13, promoting the formation of the pollution event. The increased RH could accelerate the hygroscopic growth of aerosols, leading to the increases in $PM_{2.5}$ concentrations (Fig. 2); meanwhile, the decreased wind speed was conducive to the accumulation of the pollutants. In the daytime of February 14, the SLP began to decrease, which was unfavorable for the diffusion of pollutants, contributing to the continuous increase in concentrations of PAN and $PM_{2.5}$. After that, the high RH, low wind speed, and decreased SLP conspired to sustain the pollution persistently, until the morning of February 16. In the morning of February 16, the northeasterly wind started to prevail with increased wind speed and SLP, and decreased RH. At that time, the concentrations in $PM_{2.5}$ and PAN reduced sharply, and the event ended.

Table 2 presents the statistical results for meteorological variables in the observed and simulated results. Generally, the features of SLP, T2, RH and wind were captured well by the model, although overestimations of T2, RH and wind speed occurred. The MB value for T2 was

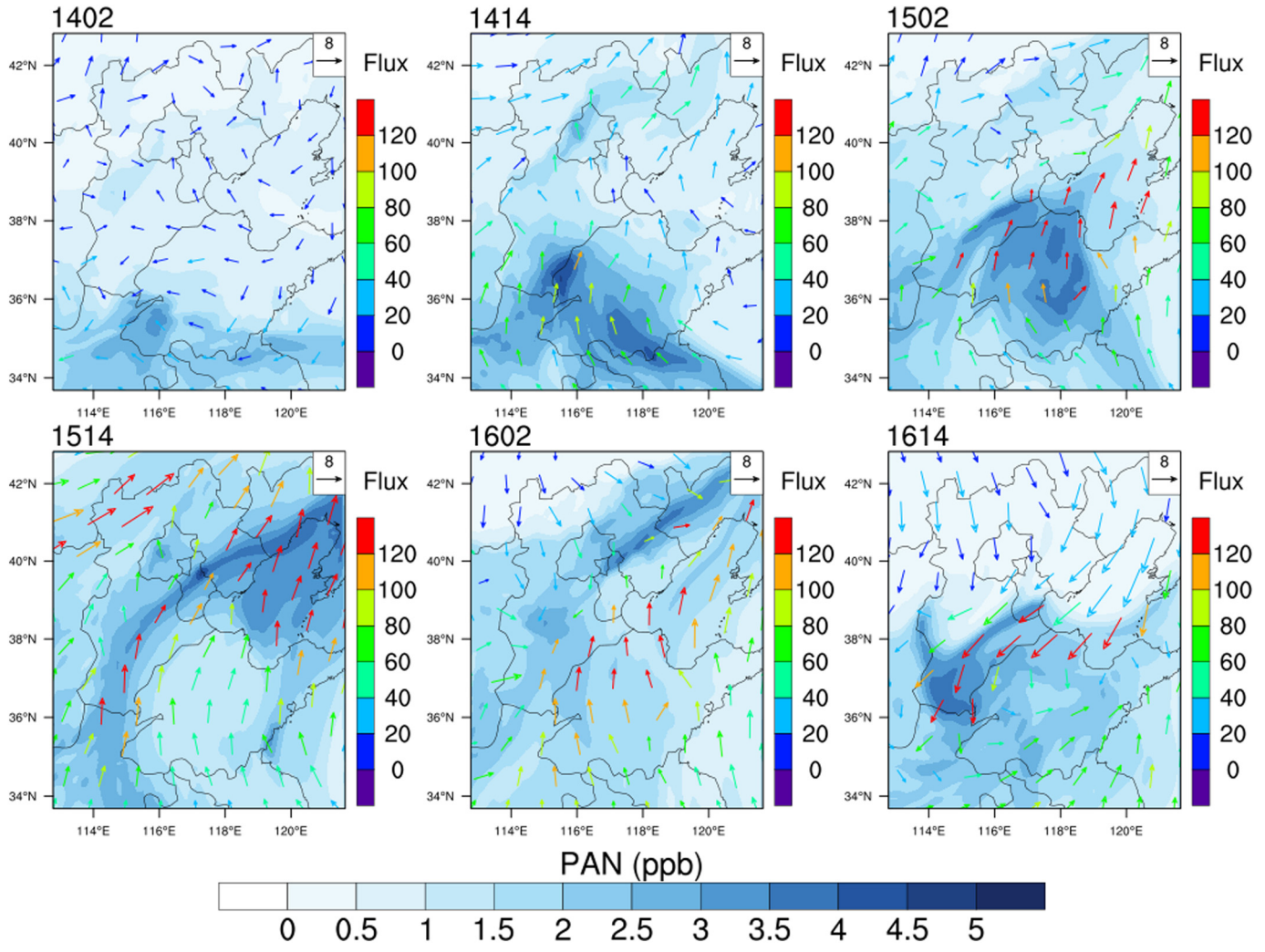

Fig. 6. Simulated spatial distributions of surface PAN concentrations (contour, ppb) and average transport flux (μg m^{-2} s^{-1}) within the 1.2 km layer above the ground in the NCP during February 14–16, 2017.

0.9 °C, which might be attributed to the lack of aerosol radiative effects. The NMB value for wind speed was 19.0%, which have been reported in previous studies using the WRF-Chem model over China and other countries (Zhang et al., 2010; Jiang et al., 2012; Situ et al., 2013). This could be caused by the default surface land cover type in WRF-Chem (Wang et al., 2012). In general, the model shows a good performance in simulating surface meteorological parameters in Beijing during this pollution event.

Except for surface meteorology, vertical distribution of temperature also has great impacts on the evolution of the pollution event (Ding et al., 2013; Wang et al., 2015). The simulated and observed 12-hourly variations of temperature profiles in Beijing during February 13–16 are displayed in Fig. S5. Results showed that the temperature inversion started to build up in the nighttime of February 13, and deepened during February 14–15, which was favorable for PAN and other pollutants to be accumulated in the boundary layer. In the morning of February 16, the inversion layer broke up and the pollution event was terminated.

The simulated south-to-north cross sections of the *v*-*w* wind and temperature in the NCP are illustrated in Fig. 5. It should be noted that Beijing (about 40°N) is located in the south edge of the Yanshan Mountain. During February 14 to 15, the NCP was dominated by the southerly wind in the boundary layer, and the wind speed decreased with latitude. This could result in the accumulation of PAN and other pollutants in Beijing and its surrounding area. Besides, the temperature inversion existed, especially during the nighttime, which also induced difficulties in vertical diffusion of pollutants. In the morning of February 16, the cold air with strong northerly wind began to dominate in Beijing, leading to the collapse of the temperature inversion.

3.4. Relative contribution of local sources and regional transport to PAN levels in Beijing

3.4.1. Horizontal and vertical distributions of PAN flux

To investigate the impact of transport on local PAN levels in Beijing below the boundary layer, we calculated the transport flux of PAN averaged within the 1.2 km above ground level during the pollution event. The choice of 1.2 km is basically consistent with previous studies about wintertime haze events of Beijing (Zhao et al., 2013; Zhang et al., 2015). The spatial distributions of simulated PAN flux and PAN concentrations in the NCP during February 14–16 are illustrated in Fig. 6. As seen from Fig. 6, the high concentration of PAN occurred in the south of the NCP region on February 14 due to the stable atmosphere in that region. Because of the prevailed southerly wind over the whole region during February 14–15, PAN with high concentrations was transported northward, coincided with the high PAN flux. On February 15, the high transport flux for PAN existed in the southeastern NCP region, which moved northward and largely influenced PAN concentrations in Beijing, especially for those in the eastern Beijing. During the daytime on February 16, the strong north wind prevailed in the NCP, and the transport flux for PAN decreased obviously.

In addition, the temporal variations of horizontal and vertical transport flux for PAN averaged within the 1.2 km above the ground in urban Beijing are shown in Fig. 7. It was illustrated that the input of the vertical transport flux for PAN in the lower troposphere existed during the polluted days (February 13–15), and showed the increasing trend with time. Besides, the horizontal flux also showed increasing trend with time during the polluted days. These could verify the great impacts of regional transport on the PAN levels in Beijing.

3.4.2. Impacts of local sources on PAN concentrations in Beijing

As shown above, the transport from the surrounding area plays an important role in the accumulation of PAN and aerosols in Beijing during the pollution event. To figure out relative contributions of local sources and transport from other regions to PAN concentrations in Beijing, sensitivity simulations were conducted. Fig. 8 displays the differences in PAN and $PM_{2.5}$ concentrations between the CTRL_CBMZ and NOBJ_CBMZ case in Beijing and the surrounding area, which represents the local source contribution. It was seen that local sources accounted for about 15%–30% of mean PAN concentrations over most of Beijing averaged over the event. However, the local contribution to $PM_{2.5}$ was much higher than that of PAN, with corresponding values of about 25%–60%, comparable with that in Li and Han (2016).

The temporal variations of local contributions to PAN and $PM_{2.5}$ concentrations in Beijing are also shown in Fig. 9. From the afternoon to the nighttime on February 13, local contributions to PAN concentrations in Beijing were decreased from 45% to below 10%, and the corresponding

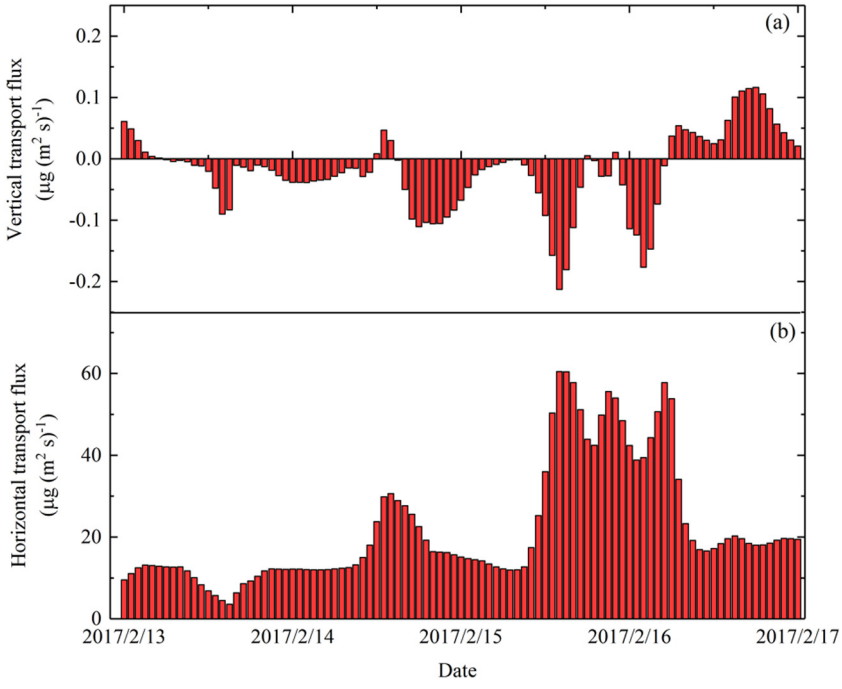

Fig. 7. Simulated time series of the vertical and horizontal transport flux (μg m^{-2} s^{-1}) averaged within the 1.2 km layer above the ground in urban Beijing during February 13–16, 2017.

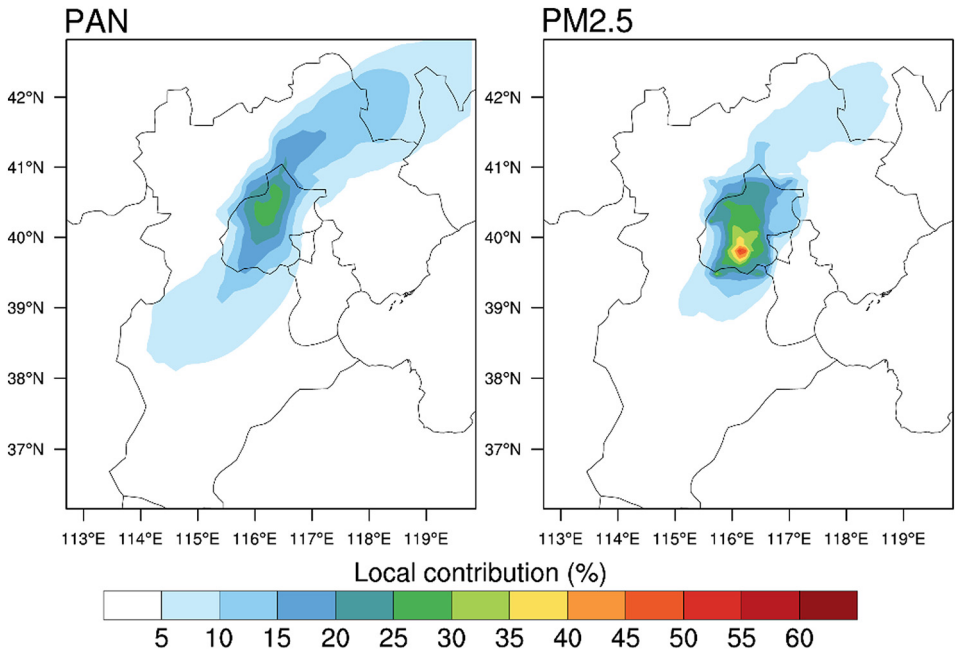

Fig. 8. Simulated spatial distributions of local source contributions to surface-layer concentrations of PAN and $PM_{2.5}$ (%) in Beijing averaged during February 13–16, 2017.

contributions to $PM_{2.5}$ concentrations were decreased from 82% to below 20%. During the polluted days, ratios of local contributions to PAN and $PM_{2.5}$ in Beijing were even below 20% and below 30%, respectively. These all confirm that during the pollution days in winter, PAN accumulation in Beijing is primarily caused by the regional transport from the surrounding areas.

As shown in Section 3.2, there is an obvious underestimation in simulated PAN concentration in the CTRL_CBMZ simulation, while such low bias can be significantly reduced by increasing VOC emissions by 20%. We further show that the simulated bias in CTRL_CBMZ marginally affects the estimated contribution of local sources and regional transport to PAN levels in Beijing. The contribution from local sources to mean PAN concentrations in Beijing is only enhanced by <5% under the condition that anthropogenic VOC emissions are increased by 20%.

4. Conclusions

In this study, variations of concentrations of PAN and other related species during a polluted event in winter of Beijing were examined using in-situ observations and the WRF-Chem model. The model performed well in reproducing the characteristics of PAN and other chemical species in winter of Beijing. Sensitivity simulation quantified the

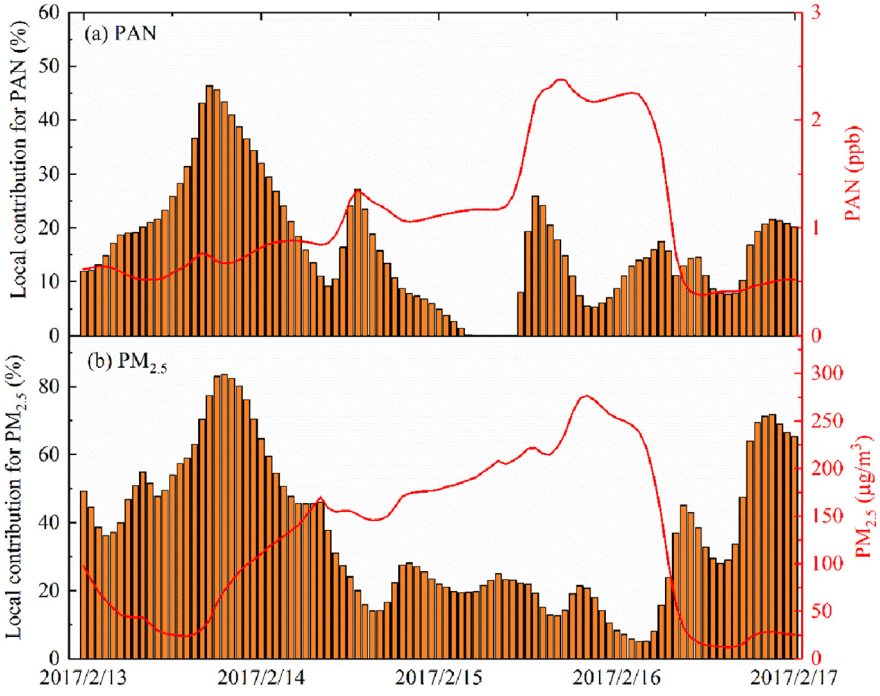

Fig. 9. Simulated time series of local source contributions to the surface-layer concentrations for PAN and $PM_{2.5}$ in Beijing during February 13–16, 2017.

relative contributions of local emission sources and regional transport to PAN levels in Beijing during the event.

During the episode on February 13–16, 2017, the observed PAN concentrations at the urban and rural sites in Beijing were 1.9 ppb and 1.7 ppb, respectively. Model evaluation showed that the WRF-Chem model reproduced the temporal features of concentrations in $PM_{2.5}$, O_3 and NO_2 well in Beijing, with *R* values of 0.90, 0.82, and 0.84, respectively. For PAN, the simulation with the CBM-Z gas scheme performed much better than simulation using the RADM2 scheme, which mainly resulted from the better representation in the reaction rates of PAN formation through $CH_3C(O)O_2$ radicals and NO_2. But the PAN concentrations in Beijing still had low bias using the CBM-Z scheme, and a sensitivity simulation with VOC emissions increased by 20% could significantly reduce the simulated low bias of PAN concentrations in Beijing.

As PAN is strongly temperature-dependent, its lifetime becomes as long as several days in winter with low temperature. Thus, it could be conducive to be accumulated and transported, like $PM_{2.5}$. Simulated results showed that the input of the vertical transport flux for PAN in the lower troposphere existed during the polluted days (February 13–15). In addition, the horizontal flux also increased with time during the polluted days. These could confirm the great impacts of regional transport on the PAN levels in Beijing. Model results also demonstrated that local sources accounted for about 15%–30% of mean PAN concentrations over most of Beijing during the event, lower than that of $PM_{2.5}$ (25%–60%). These imply that during the pollution days in winter, PAN accumulation in Beijing is primarily resulted from the regional transport from the surrounding areas. These will cause more health concerns, and its control strategies need larger regional efforts than those conducted for $PM_{2.5}$.

Acknowledgements

The authors would like to thank the staff of the Shangdianzi station for their excellent work. This research is supported by the National Key R&D Program of China [Grant Number: 2016YFC0201902], the National Science Foundation of China [Grant Number: 41475135], and the Key Laboratory of Atmospheric Chemistry, China Meteorological Administration [Grant Number: 2017B04]. All of the observational data and WRF-Chem model results have been archived by the corresponding author, Prof. Zhiqiang Ma (zqma@ium.cn), and are available upon request.

Appendix A. Supplementary data

Supplementary data to this article can be found online at https://doi.org/10.1016/j.scitotenv.2018.09.253.

References

Ackermann, I.J., Hass, H., Memmesheimer, M., Ebel, A., Binkowski, F.S., Shankar, U., 1998. Modal aerosol dynamics model for Europe: development and first applications. Atmos. Environ. 32, 2981–2999.

Beine, H., Krognes, T., 2000. The seasonal cycle of peroxyacetyl nitrate (PAN) in the European Arctic. Atmos. Environ. 34, 933–940.

Binkowski, F.S., Shankar, U., 1995. The regional particulate matter model: 1. Model description and preliminary results. J. Geophys. Res. 100, 26191–26209. https://doi.org/10.1029/95JD02093.

Cai, W., Li, K., Liao, H., Wang, H., Wu, L., 2017. Weather conditions conducive to Beijing severe haze more frequent under climate change. Nat. Clim. Chang. 7, 257–263. https://doi.org/10.1038/NCLIMATE3249.

Chapman, E.G., Gustafson, W.I., Easter, R.C., Barnard, J.C., Ghan, S.J., Pekour, M.S., Fast, J.D., 2009. Coupling aerosol-cloud-radiative processes in the WRF-Chem model: investigating the radiative impact of elevated point sources. Atmos. Chem. Phys. 9, 945–964. https://doi.org/10.5194/acp-9-945-2009.

Chou, M.-D., Suarez, M.J., Ho, C.-H., Yan, M.M.H., Lee, K.-T., 1998. Parameterizations for cloud overlapping and shortwave single-scattering properties for use in general circulation and cloud ensemble models. J. Clim. 11, 202–214. https://doi.org/10.1175/1520-0442(1998)011<0202:PFCOAS>2.0.CO;2.

Ding, A.J., Fu, C.B., Yang, X.Q., et al., 2013. Intense atmospheric pollution modifies weather: a case of mixed biomass burning with fossil fuel combustion pollution in eastern China. Atmos. Chem. Phys. 13 (20), 10545–10554.

Ding, A.J., et al., 2016. Enhanced haze pollution by black carbon in megacities in China. Geophys. Res. Lett. 43, 2873–2879. https://doi.org/10.1002/2016GL067745.

Emmons, L.K., Walters, S., Hess, P.G., Lamarque, J.F., Pfister, G.G., Fillmore, D., Granier, C., Guenther, A., Kinnison, D., Laepple, T., Orlando, J., Tie, X., Tyndall, G., Wiedinmyer, C., Baughcum, S.L., Kloster, S., 2010. Description and evaluation of the model for ozone and related chemical tracers, version 4 (MOZART-4). Geosci. Model Dev. 3, 43–67.

Fast, J.D., Gustafson, W.I., Easter, R.C., Zaveri, R.A., Barnard, J.C., Chapman, E.G., Grell, G.A., Peckham, S.E., 2006. Evolution of ozone, particulates, and aerosol direct radiative forcing in the vicinity of Houston using a fully coupled meteorology-chemistry-aerosol model. J. Geophys. Res. 111, D21305. https://doi.org/10.1029/2005JD006721.

Fischer, E.V., Jacob, D.J., Yantosca, R.M., Sulprizio, M.P., Millet, D.B., Mao, J., Paulot, F., Singh, H.B., Roiger, A., Ries, L., Talbot, R.W., Dzepina, K., Pandey Deolal, S., 2014. Atmospheric peroxyacetyl nitrate (PAN): a global budget and source attribution. Atmos. Chem. Phys. 14, 2679–2698. https://doi.org/10.5194/acp-14-2679-2014.

Gao, Y., Zhao, C., Liu, X.H., Zhang, M.G., Leung, L.R., 2014. WRF-Chem simulations of aerosols and anthropogenic aerosol radiative forcing in East Asia. Atmos. Environ. 92, 250–266. https://doi.org/10.1016/j.atmosenv.2014.04.038.

Gao, Y., Zhang, M., Liu, Z., Wang, L., Wang, P., Xia, X., Tao, M., Zhu, L., 2015. Modeling the feedback between aerosol and meteorological variables in the atmospheric boundary layer during a severe fog-haze event over the North China Plain. Atmos. Chem. Phys. 15, 4279–4295. https://doi.org/10.5194/acp-15-4279-2015.

Gao, M., Carmichael, G.R., Wang, Y., Saide, P.E., Yu, M., Xin, J., Liu, Z., Wang, Z., 2016. Modeling study of the 2010 regional haze event in the North China Plain. Atmos. Chem. Phys. 16, 1673–1691. https://doi.org/10.5194/acp-16-1673-2016.

Grell, G.A., Peckham, S.E., Schmitz, R., McKeen, S.A., Frost, G., Skamarock, W.C., Eder, B., 2005. Fully coupled "online" chemistry within the WRF model. Atmos. Environ. 39, 6957–6975. https://doi.org/10.1016/j.atmosenv.2005.04.027.

Guenther, A., Karl, T., Harley, P., Wiedinmyer, C., Palmer, P.I., Geron, C., 2006. Estimates of global terrestrial isoprene emissions using MEGAN (Model of Emissions of Gases and Aerosols from Nature). Atmos. Chem. Phys. 6, 3181–3210.

Heuss, J.M., Glasson, W.A., 1968. Hydrocarbon reactivity and eye irritation. Environ. Sci. Technol. 2 (12), 1109–1116.

Hong, S.Y., Lim, J.J., 2006. The WRF single-moment 6-class microphysics scheme. J. Kor. Meteorol. Soc. 42, 129–151.

Hong, S.Y., Noh, Y., Dudhia, J., 2006. A new vertical diffusion package with an explicit treatment of entrainment processes. Mon. Weather Rev. 134, 2318–2341. https://doi.org/10.1175/MWR3199.1.

Hudman, R.C., Jacob, D.J., Cooper, O.R., et al., 2004. Ozone production in transpacific Asian pollution plumes and implications for ozone air quality in California. J. Geophys. Res. 109. https://doi.org/10.1029/2004JD004974.

Jiang, F., Zhou, P., Liu, Q., Wang, T., Zhuang, B., Wang, X., 2012. Modeling tropospheric ozone formation over East China in springtime. J. Atmos. Chem. 69, 303–319. https://doi.org/10.1007/s10874-012-9244-3.

Li, J., Han, Z., 2016. A modeling study of severe winter haze events in Beijing and its neighboring regions. Atmos. Res. 170, 87–97.

Li, M., Zhang, Q., Streets, D.G., He, K.B., Cheng, Y.F., Emmons, L.K., Huo, H., Kang, S.C., Lu, Z., Shao, M., Su, H., Yu, X., Zhang, Y., 2014. Mapping Asian anthropogenic emissions of non-methane volatile organic compounds to multiple chemical mechanisms. Atmos. Chem. Phys. 14, 5617–5638. https://doi.org/10.5194/acp-14-5617-2014.

Li, K., Liao, H., Cai, W.J., Yang, Y., 2018. Attribution of anthropogenic influence on atmospheric patterns conducive to recent most severe haze over eastern China. Geophys. Res. Lett. 45 (4), 2072–2081. https://doi.org/10.1002/2017GL076570.

Liu, F., Zhang, Q., Tong, D., Zheng, B., Li, M., Huo, H., He, K.B., 2015. High-resolution inventory of technologies, activities, and emissions of coal-fired power plants in China from 1990 to 2010. Atmos. Chem. Phys. 15, 13299–13317. https://doi.org/10.5194/acp-15-13299-2015.

Liu, Z., Wang, Y., Bo, H., Ji, D., Zhang, J., Wu, F., et al., 2016. Source appointment of fine particle number and volume concentration during severe haze pollution in Beijing in January 2013. Environ. Sci. Pollut. Res. Int. 23 (7), 6845–6860.

Ma, Z., Xu, J., Quan, W., Zhang, Z., Lin, W., Xu, X., 2016. Significant increase of surface ozone at a rural site, north of eastern China. Atmos. Chem. Phys. 16 (6), 3969–3977.

Mlawer, E.J., Taubman, S.J., Brown, P.D., Iacono, M.J., Clough, S.A., 1997. Radiative transfer for inhomogeneous atmospheres: RRTM, a validated correlated-k model for the longwave. J. Geophys. Res. Atmos. 102, 16663–16682.

Nielsen, T., Samuelsson, U., Grennfelt, P., Thomsen, E.L., 1981. Peroxyacetyl nitrate in long-range transported polluted air. Nature 293 (15), 553–555.

Qiu, Y., Liao, H., Zhang, R., Hu, J., 2017. Simulated impacts of direct radiative effects of scattering and absorbing aerosols on surface layer aerosol concentrations in China during a heavily polluted event in February 2014. J. Geophys. Res. Atmos. 122, 5955–5975. https://doi.org/10.1002/2016JD026309.

Sander, S.P., Friedl, R.R., Golden, D.M., et al., 2006. Chemical kinetics and photochemical data for use in atmospheric studies evaluation number 15. Jet Propulsion Laboratory Publication 06-2.

Schell, B., Ackermann, I.J., Hass, H., Binkowski, F.S., Ebel, A., 2001. Modeling the formation of secondary organic aerosol within a comprehensive air quality model system. J. Geophys. Res. Atmos. 106, 28275–28293.

Seinfeld, J.H., Pandis, S.N., 2006. Atmospheric Chemistry and Physics: From Air Pollution to Climate Change. John Wiley & Sons Inc.

Singh, H.B., Salas, L.J., 1989. Measurements of peroxyacetyl nitrate (PAN) and peroxypropionyl nitrate (PPN) at selected urban, rural and remote sites. Atmos. Environ. 23 (1), 231–238.

Singh, H.B., Salas, L.J., Viezee, W., 1986. Global distribution of peroxyacetyl nitrate. Nature 321 (5), 588–591.

Singh, H.B., Hara, D.O., Herlth, D., 1992. Atmospheric measurements of peroxyacetyl nitrate and other organic nitrates at high latitudes: possible sources and sinks. J. Geophys. Res. 97, 16511–16522.
Singh, H.B., Salas, L., Herlth, D., Kolyer, R., Czech, E., Avery, M., Crawford, J.H., Pierce, R.B., Sachse, G.W., Blake, D.R., Cohen, R.C., Bertram, T.H., Perring, A., Wooldridge, P.J., Dibb, J., Huey, G., Hudman, R.C., Turquety, S., Emmons, L.K., Flocke, F., Tang, Y., Carmichael, G.R., Horowitz, L.W., 2007. Reactive nitrogen distribution and partitioning in the North American troposphere and lowermost stratosphere. J. Geophys. Res. 112, D12S04. https://doi.org/10.1029/2006JD007664.
Situ, S., Guenther, A., Wang, X., Jiang, X., Turnipseed, A., Wu, Z., Bai, J., Wang, X., 2013. Impacts of seasonal and regional variability in biogenic VOC emissions on surface ozone in the Pearl River delta region, China. Atmos. Chem. Phys. 13, 11803–11817. https://doi.org/10.5194/acp-13-11803-2013.
Stephens, E.R., 1969. The formation, reactions and properties of peroxyacyl nitrates (PANs) in photochemical air pollution. Adv. Environ. Sci. 1, 119–146.
Stockwell, W.R., Middleton, P., Chang, J.S., 1990. The second generation regional acid deposition model: chemical mechanism for regional air quality modeling. J. Geophys. Res. 95, 16343–16367.
Sudo, K., Takahashi, M., Akimoto, H., 2002. CHASER: a global chemical model of the troposphere 2. Model results and evaluation. J. Geophys. Res. 107, 4586. https://doi.org/10.1029/2001jd001114.
Sun, Y.L., Chen, C., Zhang, Y., Xu, W., Zhou, L., Cheng, X., Zheng, H., Ji, D., Li, J., Tang, X., Fu, P., Wang, Z., 2016. Rapid formation and evolution of an extreme haze episode in Northern China during winter 2015. Sci. Rep. 6, 27151. https://doi.org/10.1038/srep27151.
Suppana, P., Fabiana, P., Vyrasa, L., Gryninga, S.E., 1998. The behaviour of ozone and peroxyacetyl nitrate concentrations for different wind regimes during the MEDCAPHOT-TRACE campaign in the greater area of Athens, Greece. Atmos. Environ. 32 (12), 2089–2102.
Taylor, O.C., 1969. Importance of peroxyacetyl nitrate (PAN) as a phytotoxic air pollutant. J. Air Pollut. Control Assoc. 19, 347–351. https://doi.org/10.1080/00022470.1969.10466498.
Temple, P.J., Taylor, O.C., 1983. World-wide ambient measurements of peroxyacetyl nitrate (PAN) and implications for plant injury. Atmos. Environ. 17 (8), 1583–1587.
Wang, B., Shao, M., Roberts, J.M., Yang, G., Yang, F., Hu, M., Zeng, L., Zhang, Y., Zhang, J., 2010. Ground-based on-line measurements of peroxyacetyl nitrate (PAN) and peroxypropionyl nitrate (PPN) in the Pearl River Delta, China. Int. J. Environ. Anal. Chem. 90 (7), 548–559.
Wang, T., Jiang, F., Deng, J., et al., 2012. Urban air quality and regional haze weather forecast for Yangtze River Delta region. Atmos. Environ. 58, 70–83. https://doi.org/10.1016/j.atmosenv.2012.01.014.
Wang, Y.S., Yao, L., Wang, L.L., Liu, Z.R., Ji, D.S., Tang, G.Q., Zhang, J.K., Sun, Y., Hu, B., Xin, J.Y., 2014. Mechanism for the formation of the January 2013 heavy haze pollution episode over central and eastern China. Sci. China Earth Sci. 57, 14–25. https://doi.org/10.1007/s11430-013-4773-4.
Wang, H., Shi, G.Y., Zhang, X.Y., et al., 2015. Mesoscale modeling study of the interactions between aerosols and pbl meteorology during a haze episode in China Jing-Jin-Ji and its near surrounding region - part 2: aerosols' radiative feedback effects. Atmos. Chem. Phys. 15, 3277–3287.
Wesely, M.L., 1989. Parameterization of surface resistance to gaseous dry deposition in regional numerical models. Atmos. Environ. 23, 1293–1304. https://doi.org/10.1016/0004-6981(89)90153-4.
Xu, Z., Xue, L., Wang, T., Xia, T., et al., 2015. Measurements of peroxyacetyl nitrate at a background site in the Pearl River delta region: production efficiency and regional transport. Aerosol Air Qual. Res. 15 (1), 833–841.
Xue, L., Wang, T., Wang, X., et al., 2014. On the use of an explicit chemical mechanism to dissect peroxyacetyl nitrate formation. Environ. Pollut. 195, 39–47.
Yang, Y., Wang, H., Smith, S.J., Ma, P.-L., Rasch, P.J., 2017a. Source attribution of black carbon and its direct radiative forcing in China. Atmos. Chem. Phys. 17, 4319–4336. https://doi.org/10.5194/acp-17-4319-2017.
Yang, Y., Russell, L.M., Lou, S., Liao, H., Guo, J., Liu, Y., Singh, B., Ghan, S.J., 2017b. Dust-wind interactions can intensify aerosol pollution over eastern China. Nat. Commun. 8, 15333. https://doi.org/10.1038/ncomms15333.
Zaveri, R.A., Peters, L.K., 1999. A new lumped structure photochemical mechanism for large-scale applications. J. Geophys. Res. 104, 30387–30415. https://doi.org/10.1029/1999JD900876.
Zaveri, R.A., Easter, R.C., Fast, J.D., Peters, L.K., 2008. Model for Simulating Aerosol Interactions and Chemistry (MOSAIC). J. Geophys. Res. 113, D13204. https://doi.org/10.1029/2007JD008782.
Zhang, Q., Streets, D.G., Carmichael, G.R., He, K.B., Huo, H., Kannari, A., Klimont, Z., Park, I.S., Reddy, S., Fu, J.S., Chen, D., Duan, L., Lei, Y., Wang, L.T., Yao, Z.L., 2009a. Asian emissions in 2006 for the NASA INTEX-B mission. Atmos. Chem. Phys. 9, 5131–5153.
Zhang, J.M., Wang, T., Ding, A.J., et al., 2009b. Continuous measurement of peroxyacetyl nitrate (PAN) in suburban and remote areas of western China. Atmos. Environ. 43 (2), 228–237.
Zhang, Y., Wen, X.Y., Jang, C.J., 2010. Simulating chemistry-aerosol-cloud-radiation-climate feedbacks over the continental US using the online-coupled Weather Research Forecasting model with chemistry (WRF/Chem). Atmos. Environ. 44, 3568–3582. https://doi.org/10.1016/j.atmosenv.2010.05.056.
Zhang, J.B., Xu, Z., Yang, G., Wang, B., 2011. Peroxyacetyl nitrate (PAN) and peroxypropionyl nitrate (PPN) in urban and suburban atmospheres of Beijing, China. Atmos. Chem. Phys. Discuss. 11, 8173–8206.
Zhang, H., Xu, X., Lin, W., Wang, Y., 2014. Wintertime peroxyacetyl nitrate (PAN) in the megacity Beijing: role of photochemical and meteorological processes. J. Environ. Sci. 26 (1), 83–96.
Zhang, L., Wang, T., Lv, M., Zhang, Q., 2015. On the severe haze in Beijing during January 2013: unraveling the effects of meteorological anomalies with WRF-Chem. Atmos. Environ. 104, 11–21.
Zhang, B., Zhao, B., Zuo, P., Huang, Z., Zhang, J., 2017. Ambient peroxyacyl nitrate concentration and regional transportation in Beijing. Atmos. Environ. 166, 543–550.
Zhang, Z., Xu, X., Qiao, L., 2018. Numerical simulations of the effects of regional topography on haze pollution in Beijing. Sci. Rep. 8 (1), 5504. https://doi.org/10.1038/s41598-018-23880-8.
Zhao, X.J., Zhao, P.S., Xu, J., Meng, W., Pu, W.W., Dong, F., He, D., Shi, Q.F., 2013. Analysis of a winter regional haze event and its formation mechanism in the North China Plain. Atmos. Chem. Phys. 13, 5685–5696.
Zheng, B., Huo, H., Zhang, Q., Yao, Z.L., Wang, X.T., Yang, X.F., Liu, H., He, K.B., 2014. High-resolution mapping of vehicle emissions in China in 2008. Atmos. Chem. Phys. 14, 9787–9805. https://doi.org/10.5194/acp-14-9787-2014.
Zheng, G., Su, H., Zhang, Q., Cheng, Y., He, K., 2015. Exploring the severe winter haze in Beijing: the impact of synoptic weather, regional transport and heterogeneous reactions. Atmos. Chem. Phys. 15 (6), 2969–2983.